INTERNATIONAL JOURNAL FOR NUMERICAL METHODS IN FLUIDS, VOL. 23, 125–142 (1996)

TOWARDS A NEW MODEL-FREE SIMULATION OF HIGH-REYNOLDS-FLOWS: LOCAL AVERAGE DIRECT NUMERICAL SIMULATION

F. M. DENARO*

Department of Energetic Thermofluidynamics and Environmental Control, University of Naples, 'Federico II', Naples, Italy

SUMMARY

Studies on the numerical simulation of high-Reynolds-number flows encounter difficulties due to the wide range of characteristic length and time scales existing in the flow field. These are often much smaller than the computational grid size. A new approach based on a 'model-free' local average direct numerical simulation is presented which incorporates a strategy to filter the non-resolvable scales by means of an integration over the domain and to recover the contribution of the subgrid scales by using an integral formulation developed for them. The resulting weak formulation allows us to define a numerical flux that, thanks to the filtering operation, is highly accurate. Several computation test-cases concerning theoretical accuracy and the Navier–Stokes equations at high Reynolds number are carried out without using any turbulence model. The obtained accuracy for all computations confirms that this approach can be considered a valid contribution in the field of direct numerical simulation.

KEY WORDS: model-free simulation; direct numerical simulation; large eddy simulation; multidimensional high-order fluxes

1. INTRODUCTION

One of the most exciting challenges of modern research in the computational fluid dynamics (CFD) field concerns the numerical simulation of transport equations at high Reynolds (or Peclet) number. It is well known that, for the still simple problem of the 1D solution of the linear wave equation, numerical simulations can be obtained by replacing the partial differential equation by a wide class of approximate numerical operators (see e.g. Reference 1). Consequently, in the resulting modified equations some terms appear which, from a mathematical point of view, vanish only if the integration steps go to zero (consistence property) or when the Courant number can be held at an adequate constant value over the whole domain. These terms are responsible for loss of accuracy when the flows (as in practical cases) have such a low physical diffusion that the numerical one totally changes their true character. This is a considerable problem in the case of Navier–Stokes equation solutions at high Reynolds number, because the characteristics of laminar, transitional and turbulent flows coexist and can be strongly biased by the real (physical plus numerical) diffusion. One of the most attractive approaches since Orszag's simulations in 1969 is the direct numerical simulation (DNS) of the transport equations owing to its 'potential capability'. DNS ideally describes the true behaviour of all the flow field scales, but to succeed with this approach, one must consider the variations in length

* Current address: Department of Aerospace Engineering, Second University of Naples, Auersa, Italy.

CCC 0271–2091/96/020125–18

Received February 1995
Revised November 1995

scales, ranging from the characteristic length of the computational domain up to the smallest eddy size where the mechanisms of energy dissipation occur. As a consequence, it is well known that at high Reynolds number the problems caused by the large number of required grid points overcome the existing computer performances for solving problems of practical interest (see e.g. Reference 2). However, some papers have shown that the grid point numbers do not always need to be as large as the theoretical assumptions require,[3–5] because the flow characteristics are generally determined by the large-scale structures. Nevertheless, the problem related to any DNS should still be stated as: *since any non-linear flow characteristic is innate in advective terms, one must use an adequate approximate (numerical) operator for them.* To determine what the term 'adequate' stands for is the objective of the present paper.

A new approach that has been studied since 1989 by the present author during the preparation of his graduation thesis[6] is described here (see e.g. References 7 and 8). In the present approach the unsteady transport equations are solved without assuming any turbulence model (as in DNS). After a prefiltering operation the contribution due to the scales not representable on a given mesh is considered in an integral form by means of an appropriate approximate reconstruction of the local transport variables. This approach results in a weak formulation that can be seen as a large-eddy simulation (LES) type of procedure, because, by means of a local averaging procedure, the small scales are filtered (as in LES) but there is no use of any explicit subgrid scale (SGS) model for the closure of the equations (and no arbitrary isotropy assumption). A direct evaluation, conceived to replace the model, is discussed. For these reasons, this approach can be considered more flexible than LES and stronger than classical DNS. To obtain this goal, a multidimensional Taylor expansion of the local solution together with a multidimensional polynomial interpolation is used. Thanks to the filtering operation, it allows us to define a numerical flux of high-order accuracy in time and space. Several 'model-free' computations at high Reynolds number are analysed and discussed.

2. THEORETICAL BACKGROUND

Let us consider the balance equation for a quantity ϕ in integral form over a fixed control volume (CV) Ω:

$$\int_\Omega \frac{\partial \phi}{\partial t} \mathrm{d}\Omega = \int_{B\Omega} \mathbf{n} \cdot \mathbf{F}(\phi) \mathrm{d}B\Omega, \tag{1}$$

where $\mathbf{F}(\phi)$ is the sum of the advective flux $\mathbf{F}_{ad} = -\mathbf{v}\phi$ ($\mathbf{v}$ is the velocity field) and the diffusive flux $\mathbf{F}_d$. By integrating over $[t, t+\Delta t]$, calling V the measure of Ω, one gets

$$[\bar{\phi}(t+\Delta t) - \bar{\phi}(t)]V = \int_t^{t+\Delta t} \left(\int_{B\Omega} \mathbf{n} \cdot \mathbf{F}(\phi) \mathrm{d}B\Omega \right) \mathrm{d}t, \tag{2}$$

with the definition of average value given by

$$\bar{\phi}(t) = \frac{1}{V} \int_\Omega \phi(\mathbf{x}, t) \mathrm{d}\Omega \equiv \int_\Omega G(\mathbf{x}, \mathbf{x}', \Delta) \phi(\mathbf{x}, t) \mathrm{d}\Omega. \tag{3}$$

This CV approach should be interpreted as a prefiltering operation (the filter G depends on the characteristic length Δ related to the measure of the CV) necessary in the sense that, by averaging the transport variables, they become 'smoother', making them representable on a given computational grid. In fact, if one solved the transport equation directly in terms of the local formulation arising from equation (1), one would fall within a classical DNS type of procedure with its well-known related problems. Instead, equation (2) can be computed with a high order of accuracy by means of a suitable

Taylor time expansion of kth order[7,8] where each time derivative is replaced via the balance equation. In this way one obtains

$$(\Delta_t\bar{\phi})V = [\bar{\phi}(t+\Delta t) - \bar{\phi}(t)]V = -\Delta t \int_{B\Omega} \mathbf{n}\cdot\mathbf{v}E_t^{(k)}\phi \mathrm{d}B\Omega + \Delta t \int_{B\Omega} \mathbf{n}\cdot\mathbf{F}_\mathrm{d}\mathrm{d}B\Omega, \tag{4}$$

where the time integration operator $E_t^{(k)}$ is defined as*

$$E_t^{(k)} \equiv \left(I + \frac{\Delta t}{2}L_\mathrm{ad} + \cdots + \frac{\Delta t^{k-1}}{k!}L_\mathrm{ad}^{(k-1)}\right), \tag{5}$$

in which $L_\mathrm{ad} = -\nabla\cdot[\mathbf{v}(\cdot)]$ is the advective operator, I is the identity operator and the power exponent in parentheses indicates a symbolic product of operators.

The second stage of this approach is the reconstruction step. In order to have a better understanding of the present approach, Figure 1 illustrates the procedure. At a point $\mathbf{x}_\mathrm{c}$ a generic transport variable ϕ can be split into two terms, an average one and a residual one:

$$\phi(\mathbf{x}_\mathrm{c}) = \bar{\phi} + \varepsilon(\mathbf{x}_\mathrm{c}) \quad \forall t \geq t_0. \tag{6}$$

By evaluating this relation at t and $t+\Delta t$, one obtains

$$\begin{aligned}\phi(\mathbf{x}_\mathrm{c}, t+\Delta t) &= \phi(\mathbf{x}_\mathrm{c}, t) + \Delta_t\bar{\phi} + \Delta_t\varepsilon \\ &\approx \phi(\mathbf{x}_\mathrm{c}, t) + \Delta_t\bar{\phi} + \left.\frac{\partial\varepsilon(\mathbf{x}_\mathrm{c})}{\partial t}\right|_t \Delta t + \cdots + \left.\frac{\partial^{K_\varepsilon}\varepsilon(\mathbf{x}_\mathrm{c})}{\partial t^{K_\varepsilon}}\right|_t \frac{\Delta t^{K_\varepsilon}}{K_\varepsilon!}.\end{aligned} \tag{7}$$

To express the residual part, a suitable Taylor space expansion (where nd is the space dimension) of mth order is adopted for the transport variable around a point $\mathbf{x}_\mathrm{c}$. By integrating such an expansion over the CV, dividing it by its measure and equating it to equation (6), one gets

$$\varepsilon(\mathbf{x}_\mathrm{c}) = R_s^{(m)}\phi. \tag{8}$$

The space reconstruction operator $R_s^{(m)}$ is defined as†

$$R_s^{(m)} \equiv -\sum_{j=1}^{m}\frac{1}{j!}\left[\frac{1}{V}\int_\Omega\left(\sum_{i=1}^{nd}(x_i - x_{ic})\left.\frac{\partial}{\partial x_i}\right|_{x_\mathrm{c}}\right)^{(j)}\mathrm{d}\Omega\right], \tag{9}$$

where the 'jth symbolic power' is obtained by taking the jth power and replacing each product of j partial derivatives by the jth derivative with respect to the variable that appears. Because of the time independence of the space reconstruction operator, one can express the time derivatives of the spatial fluctuation ε as

$$\left.\frac{\partial^j\varepsilon(\mathbf{x}_\mathrm{c})}{\partial t^j}\right|_t = R_s^{(m)}\left.\frac{\partial^j\phi}{\partial t^j}\right|_t \quad (j = 1, \ldots, K_\varepsilon). \tag{10}$$

---

* It can be easily shown that

$$\frac{1}{\Delta t}\int_t^{t+\Delta t}\mathbf{F}_\mathrm{ad}\mathrm{d}t = \langle\mathbf{F}_\mathrm{ad}\rangle = -\mathbf{v}E_t^{(k)}\phi,$$

so that by means of the time integration operator the advective flux results in being time averaged, i.e. one has a prefiltering operation with respect to the time too.

† It is worth noting that the structure of ε contains terms (such as gradients and curvatures) which allow us to recover the behaviour of the transported quantity during any time step. Such terms, being related to odd and even derivatives, are necessary to improve diffusion and dispersion errors.

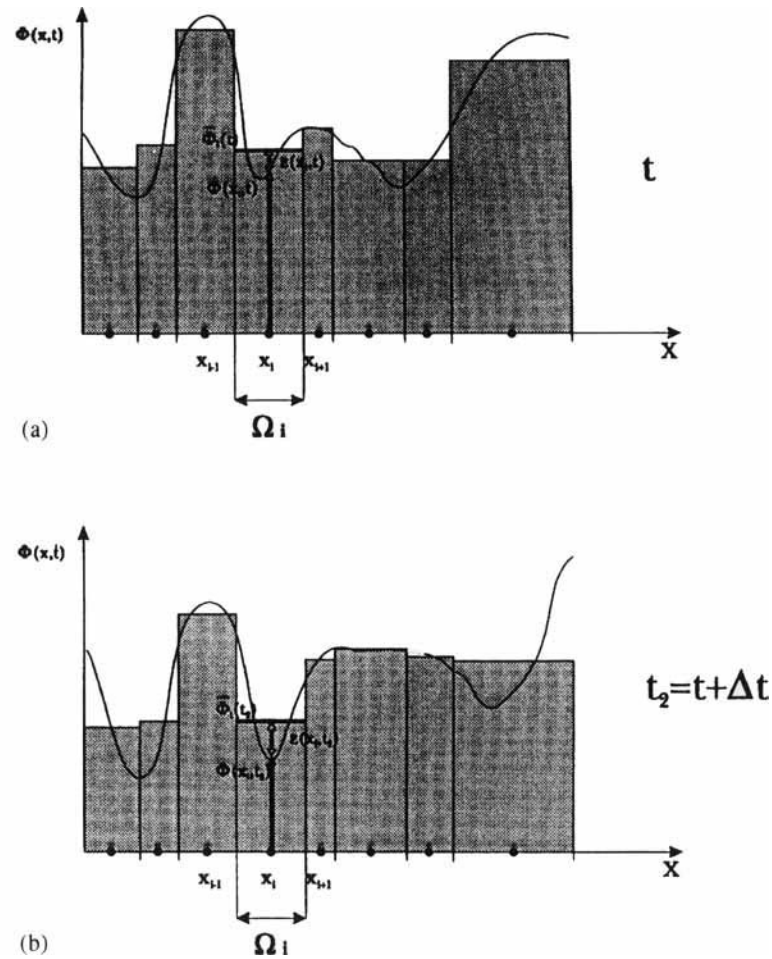

Figure 1. Sketch of present CV approach. Step (a): the set of local values $\phi(x_i, t)$ is known as well as, by means of polynomial interpolation, the average values. Step (b): at time $t + \Delta t$ the average values are computed from equation (4) and the local values $\phi(x_i, t + \Delta t)$ are reconstructed from the evaluation of equation (11)

Now, by substituting the local balance equation in which one neglects the diffusive contribution (this is because of the high-Reynolds-number hypothesis, but it can easily be removed in general), inverting the order between divergence and space reconstruction operators and applying some mathematical theorems,[8] one gets

$$\Delta_t \varepsilon = -\frac{\Delta t}{V} \int_{B\Omega} \mathbf{n} \cdot R_s^{(m)}(\mathbf{v} E_t^{(k_\varepsilon)} \phi) \mathrm{d}B\Omega. \tag{11}$$

Finally, by substituting equations (4) and (11) into equation (7), the latter can be rewritten as

$$\phi(\mathbf{x}_c, t + \Delta t) = \phi(\mathbf{x}_c, t) + \frac{\Delta t}{V} \left(\int_{B\Omega} \mathbf{n} \cdot \mathbf{F}_{\mathrm{ad}}^{(k,k_\varepsilon,m)} \mathrm{d}B\Omega + \int_{B\Omega} \mathbf{n} \cdot \mathbf{F}_{\mathrm{d}} \mathrm{d}B\Omega \right), \tag{12}$$

where the 'reconstructed' high-order advective flux is defined as

$$\mathbf{F}_{\mathrm{ad}}^{(k,k_\varepsilon,m)} = -(\mathbf{v}E_t^{(k)} + R_s^{(m)}\mathbf{v}E_t^{(k_\varepsilon)})\phi. \tag{13}$$

In conclusion, referring to equation (7), one can write

> new pointwise value =old pointwise value + time contribution of Local Average
> + time contribution of residual part of ϕ,

so that one can summarize that the idea of this approach is to reconstruct the pointwise value by adding equation (11) to the local average contribution given by equation (4) (well computed by means of the filtering operation), where equation (11) should be interpreted as an additional 'integral balance equation for the subgrid scales'. In this framework this approach can be interpreted as an intermediate one between LES (with a 'model-free subgrid closure') and DNS.

3. NUMERICAL SCHEME

Let us define a partition of the domain Ω into a set of N subdomains Ω_i surrounding the points $\mathbf{x}_i$ so that

$$\{\Omega_i\}\colon\ \Omega = \bigcup_{i=1}^{N} \Omega_i, \qquad \Omega_i \bigcap \Omega_j = \{0\} \quad \forall i \neq j.$$

Moreover, b_i is the number of boundaries of Ω_i and $\mathbf{n}_l$ is the normal to the lth boundary in the outward direction. For each boundary $B\Omega_{il}$ we define a local multidimensional polynomial interpolation based on pointwise values. This means that for each variable $(\cdot)$ one defines a polynomial of degree $g_{(\cdot)}$ so that

$$\phi(\mathbf{x},t) \approx \phi_l^{g_\phi}(\mathbf{x},t) = \mathbf{C}_\phi^{\mathrm{T}} \cdot \mathbf{B}_\phi, \qquad \mathbf{v}(\mathbf{x},t) \approx \mathbf{v}_l^{g_\mathbf{v}}(\mathbf{x},t) = \mathbf{C}_\mathbf{v}^{\mathrm{T}} \cdot \mathbf{B}_\mathbf{v}, \qquad E_{t_l}^{(k)} \approx \hat{E}_{t_l}^{(k,g_\mathbf{v})}, \tag{14}$$

where the 'hat' indicates the approximate discrete operator of the corresponding differential one. The terms $\mathbf{C}_{(\cdot)}$ and $\mathbf{B}_{(\cdot)}$ are vectors of $r_{g_{(\cdot)}}$ elements.* Thus we can approximate equation (13) on each boundary $B\Omega_{il}$ as

$$\mathbf{F}_{\mathrm{ad}_l}^{(k,k_\varepsilon,m)} \approx \hat{\mathbf{F}}_{\mathrm{ad}_l}^{(k,k_\varepsilon,m,g_\phi,g_\mathbf{v})} = -(\mathbf{v}_l^{g_\mathbf{v}}\hat{E}_{t_l}^{(k,g_\mathbf{v})} + \hat{R}_{s_l}^{(m)}\mathbf{v}_l^{g_\mathbf{v}}\hat{E}_{t_l}^{(k_\varepsilon,g_\mathbf{v})})\phi_l^{g_\phi}. \tag{15}$$

Then, by means of analytical or numerical integration along the boundary, one gets

$$\int_{B\Omega_i} \mathbf{n}\cdot\mathbf{F}_{\mathrm{ad}}^{(k,k_\varepsilon,m)}\,\mathrm{d}B\Omega_i \approx \sum_{l=1}^{b_i} \mathscr{F}_{\mathrm{ad}_l}(\mathbf{n}_i, \hat{\mathbf{F}}_{\mathrm{ad}_l}^{(k,k_\varepsilon,m,g_\phi,g_\mathbf{v})}, \Delta t, \ldots); \tag{16}$$

likewise, for the diffusive terms,

$$\int_{B\Omega_i} \mathbf{n}\cdot\mathbf{F}_{\mathrm{d}}\,\mathrm{d}B\Omega_i \approx \sum_{l=1}^{b_i} \mathscr{F}_{\mathrm{d}_l}(\mathbf{n}_i, \hat{\mathbf{F}}_{\mathrm{d}_l}^{(g_{\mathbf{F}_\mathrm{d}})}, \ldots). \tag{17}$$

* The value of r_g depends on the degree of the polynomial and on the space dimension nd. For example, if $nd=3$, one gets $r_g=(g+1)(g+2)(g+3)/6$.

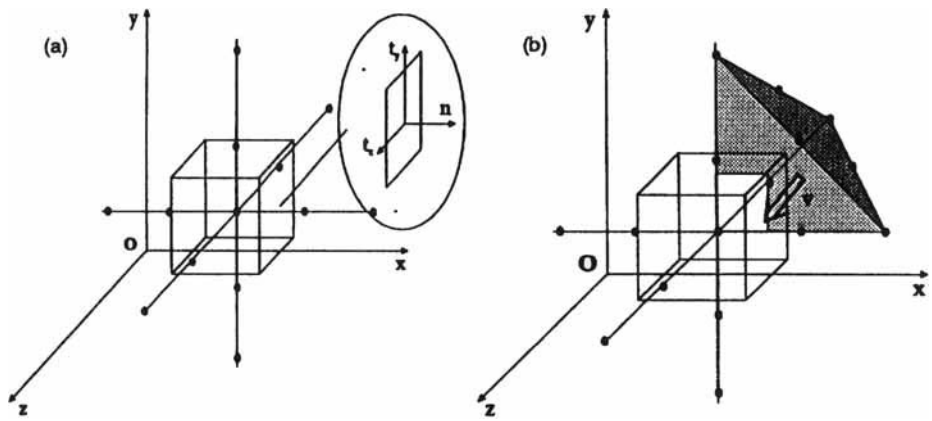

Figure 2. (a) Control volume definition on 3D structured grid. (b) Definition of adopted upwind criterion on 3D structured grid in case of $\mathbf{v}\cdot\mathbf{n}<0$, $\mathbf{v}\cdot\mathbf{t}_y<0$ and $\mathbf{v}\cdot\mathbf{t}_z>0$. Region for a complete second-degree polynomial

A fundamental observation is that such a reconstruction leads us to define a continuous flux function across each boundary.* Finally, the time-marching single-step scheme arising from equation (12) can be written as

$$\phi(\mathbf{x}_i, t+\Delta t) = \phi(\mathbf{x}_i, t) + \frac{\Delta t}{V_i}\sum_{l=1}^{b_i}(\mathscr{F}_{\mathrm{ad}_l} + \mathscr{F}_{\mathrm{d}_l}). \tag{18}$$

This scheme clearly depends on the choice of polynomials. Each polynomial is defined by imposing the pointwise values on an appropriate set of nodal points chosen to respect the 'upwind criterion' illustrated in Figure 2 for a 3D structured grid (see Reference 7 for the stability analysis).

4. RESULTS

To apply this scheme, $g_\phi = 2$ has been adopted, whilst the polynomials for the other variables have been chosen depending on the problem.† For all the following computations, $k=3$, $k_\varepsilon=1$ and $m=2$ were fixed. Several computations of test-cases are presented in the following subsections.

4.1. Scalar advection test-cases. Theoretical order of accuracy

The test-cases consist of the numerical solution of the linear advective equation with an assigned velocity field. The linear problem, even in its simplicity, retains many fundamental problems of the numerical computation and is feasible for the estimation of the accuracy of a given scheme. This seems to be a reasonable first step in order to approach flow problems at high Reynolds number. Moreover, it is useful to test the effects of the filtering operation for several types of CV in order to clarify the anisotropy effects introduced by the grid as well as the computational effort. For this goal, two test-cases were chosen from the literature.

* Many schemes use a Riemann solver to compute the flux function owing to the fact that across a boundary the reconstructed flux function is not continuous.

† It is worth remarking that schemes with quadratic interpolations (QUICKEST) were presented by Leonard[9] and Leonard and Niknafs.[10]

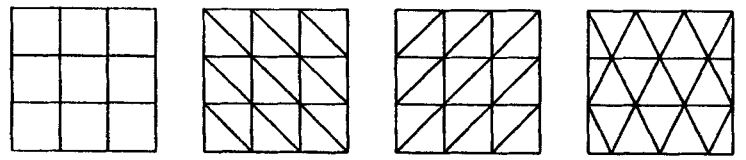

Figure 3. Test grids

1. A smooth test function is advected by a velocity field corresponding to a clockwise rigid rotation around the origin; the computation is repeated until the steady state.[11]
2. A periodic test function is advected by a uniform velocity field; the computation is repeated until $t = 2$.[12]

These test-cases were carried out on meshes of the type described in Figure 3 for various numbers of points along the x- direction: 10, 20, 30, 40 and 50. The error estimation is in the L_2-norm for the first test-case and in the L_∞-norm for the second. The resulting order of accuracy, obtained by means of a linear regression from the curve representing the error as a function of the mesh size on a double-logarithmic scale, is reported in Table I. These values show a better behaviour than both those of fourth-order ENO schemes (the order of accuracy is estimated as about 3·1 by Casper and Atkins[12]), especially in the case of the hexagonal grid, and those indicated by Deconinck *et al.*[11] for several types of schemes (Lax–Wendroff, SUPG, PSI, etc., where the obtained order of accuracy is always $\leqslant 2$). The order of accuracy of the present scheme seems to confirm that the reconstructed advective flux retains the kth order of accuracy with $g = k - 1$.

4.2. *Incompressible flows*

The computations of incompressible flows are carried out on uniform structured grids and the elliptical equation (for both streamfunction and pressure) is solved using an optimized SOR procedure.

4.2.1. Two- and three-dimensional lid-driven cavity. This is the one of the most popular test-cases for the incompressible Navier–Stokes equations (see e.g. References 13 and 14), basically owing to the simple geometry. For 2D flows a streamfunction–vorticity formulation has been used. It is worth noting that since the preparation of his graduation thesis,[6] the present author has found steady 2D solutions only for a Reynolds number $Re < 10^4$. In fact, transition to a periodic solution occurs, as was shown by de Felice *et al.*[7] In Figure 4 the streamline patterns at $Re = 7500$ computed on a 50 × 50 grid are reported. This solution, obtained on a relatively coarse grid, is practically coincident (both qualitatively and quantitatively in terms of streamfunction values) with the solution obtained by Ghia *et al.*[13] on a much more refined grid (256 × 256).

A three-dimensional computation was carried out at $Re = 3200$ on a 32 × 32 × 32 grid using a primitive variable formulation. By distributing a set of particles at a given time and following their dynamics in the flow field by solving the motion equations, the particle distribution reported in Figure 5 was obtained. In contrast with the 2D case, for the 3D lid-driven cavity some oscillations of the flow

Table I. Theoretical order of accuracy

	Structured grid	Left diagonals grid	Right diagonals grid	Hexagonal grid
Test-case 1	2·865	2·449	2·525	2·309
Test-case 2	2·979	2·954	3·158	3·675

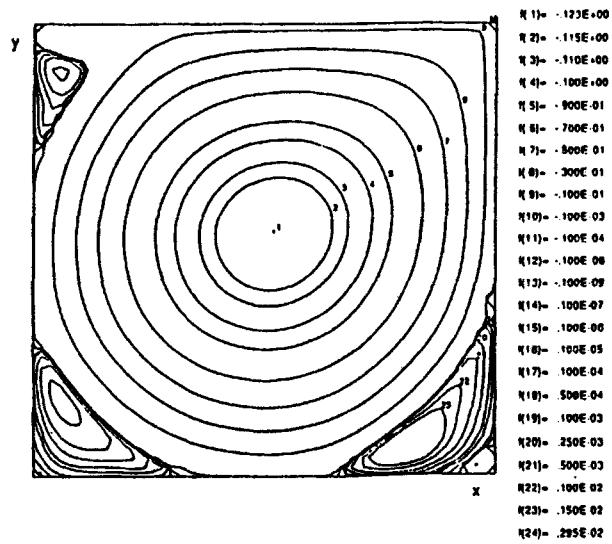

Figure 4. 2D lid-driven cavity at $Re = 7500$. Streamline pattern

variables seem to occur for this Reynolds number. This has been a subject of investigation in several previous papers (see e.g. Reference 14) in order to clarify whether a 2D simulation is realistic at such a Reynolds number.

For a given grid the computation time (herein the computations were performed on an IBM RISC 6000-320) depends on the Reynolds number. For example, a 2D steady solution at $Re = 10^3$ requires about 1 h at a Courant number of 0·5 on a 50 × 50 grid. The computation at $Re = 10^4$ requires about 4 h for a fully developed periodic solution. Of course, the 3D case is more expensive and requires about 20 h of computation. Basically, these computation times depend on the elliptical equation solver rather than on the high-order advective scheme, which, in comparison, requires a computational effort about seven times greater than the classical first-order upwind scheme, where the use of first- order upwind schemes requires a much more refined grid.

4.2.2. Two-dimensional backward-facing step. The backward-facing step represents a good and widely studied test (see e.g. References 15 and 16) owing to the laminar, transitional and turbulent character of the flow at different Reynolds numbers. Experimental investigations found that the flow becomes 3D in the transitional regime ($600 < Re < 6000$). For this reason, numerical simulations for laminar flow are at $Re = 600$ and for turbulent flow at $Re = 6 \times 10^4$. A primitive variable formulation has been used. For $Re = 600$ (360 × 30 grid points) the steady solution provides a non-dimensional reattachment length of 12·5, while the secondary region has a detachment length of 10 and a reattachment length of 20·2 (see Figure 6(a)). These values agree with those of the experimental investigations by Armaly *et al.*[15] For $Re = 6 \times 10^4$ (480 × 60 grid points) the flow field is unsteady and the reattachment point moves up and down (see Figures 6(b)–6(d)) with an average value estimated (by means of time integration) as 8·2 (Figure 6(e)). This value can be successfully compared with that of both experimental simulations and LES, from which the value of 8 is estimated to be practically constant at high Reynolds number (i.e. $Re > 10^4$). Streaklines (Figure 6(f)) are obtained by injecting a set of particles at some station of the inflow section. The plot of the vorticity time evolution at the midpoint of the outflow section (Figure 7) shows the existence of a wide range of frequencies. This fact must be emphasized, because several computations performed by the present author using other lower-

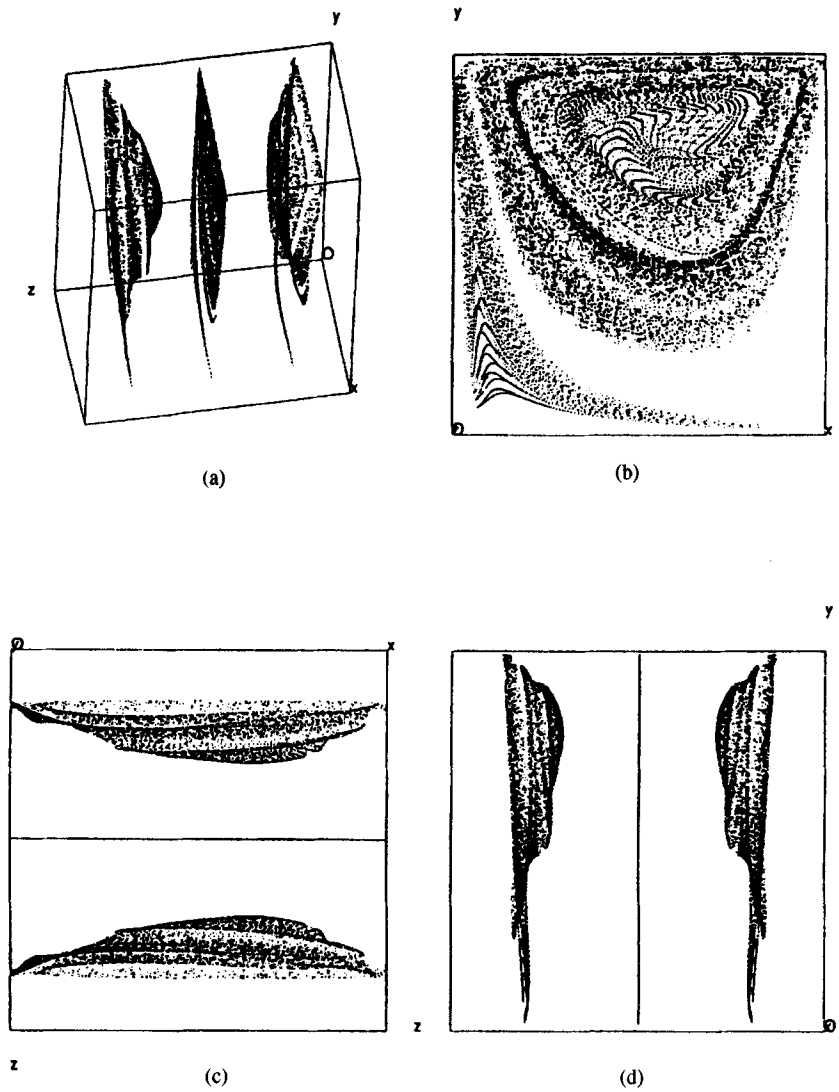

Figure 5. 3D lid-driven cavity at $Re = 3200$. Several views of particle distribution

order schemes proved that such an unsteady behaviour at high Reynolds number was not present. In fact, computations made with the first-order upwind scheme lead to an unphysical steady state (due to the large numerical diffusion) with a considerably smaller reattachment length. On the other hand, some computations made with the present scheme but without using the reconstruction operator, i.e. $m = 0$, have shown results (not reported here) that are qualitatively quite similar to the present ones but less accurate in terms of the reattachment length. This is probably due to the effects of the dispersion (phase) errors (the reconstruction operator with $m = 2$ takes into account third-order terms). Finally, it is observed that the computation time was about 40 h (including streakline computation) for a fully developed unsteady solution.

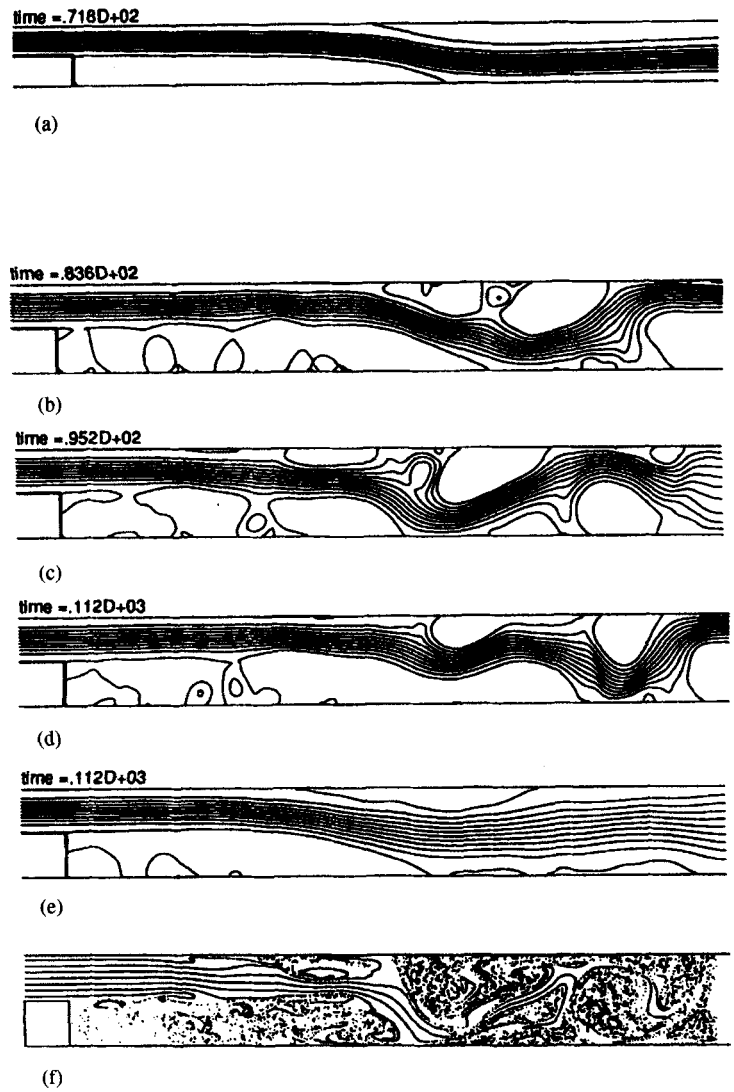

Figure 6. Backward-facing step. (a) Streamlines at $Re = 600$. (b)–(d) Instantaneous streamline patterns. (e) Averaged streamline pattern and (f) streaklines at $Re = 6 \times 10^4$

4.2.3. Two-dimensional evolving mixing layer. This test is mainly devoted to the study of mixing phenomena in a spatially evolving mixing layer. The study was performed both experimentally and numerically in order to investigate a model able to realize a quasi-periodical, unsteady flow field starting from well-defined laminar conditions. In fact, a simple Cartesian geometry was used for confinement of the flow. It consists of a main channel with a geometrical aspect ratio of 1 : 2 whose inflow section is subdivided into 32 smaller channels each having a spanwise dimension of 5 mm, where Poiseuille conditions were imposed. The central channel can guide the fluid at a different flow rate with respect to the external ones. Owing to the fluid dynamic instability mechanism (first appearing as the roll- up effect and afterwards as the pairing effect), these flows can share some properties with fully turbulent 3D flows, e.g. the presence of recognizable structures, which of course

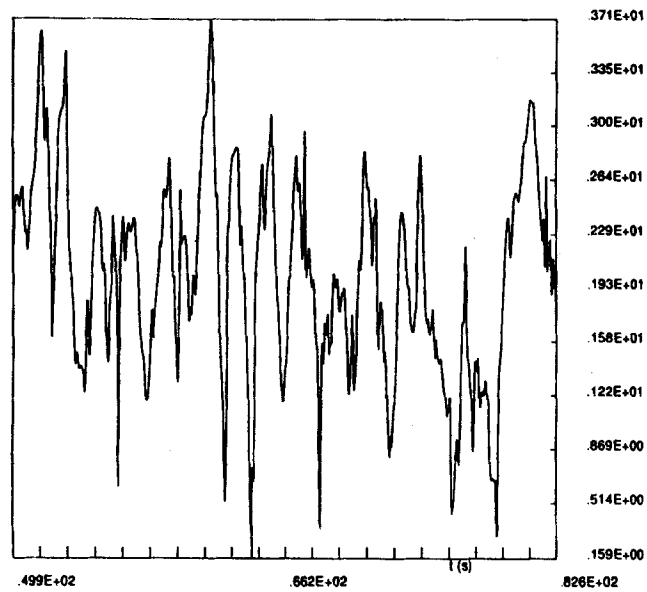

Figure 7. Backward-facing step at $Re = 6 \times 10^4$. Time evolution of vorticity at midpoint of outlet section

in 3D flows occur on a broader spectrum of length and time scales. Numerical flow visualization of the mixing phenomena has been carried out and compared with the corresponding experimental patterns.[17] A streamfunction–vorticity formulation has been adopted on a 192 × 96 grid. In Figure 8 the experimental and numerical patterns of the streaklines are shown for several flow rates. It appears that the unsteady numerical solutions (each one obtained in about 24 h) agree well with the experimental flow patterns. Studies are in progress to obtain several quantitative comparisons that are necessary to evaluate some characteristic quantities of mixing processes.

4.2.4. Flow over a flat plane with a transversal injection. Study on mechanisms of drag reduction. This study was carried out by adopting a streamfunction–vorticity formulation on a 240 × 80 grid in order to investigate the effects caused by a slot injection on a flat plate in terms of drag reduction.[18] The Reynolds number referred to the slot length (whose measure is only one mesh size) is 200. In fact, the induced separation region moves down along the plane (Figure 9(a)), thus reducing the stress on the wall. The time evolution of the total drag is shown in Figure 9(b), while in Figure 9(c) the time evolution of the average time integral of the total drag shows the diminishment of the drag when the flow becomes fully unsteady. Experimental investigations (still in progress) confirmed this mechanism of drag reduction.

4.2.5. Axisymmetric rotating–heated cavity. The last test for incompressible flow is the motion in an axisymmetric rotating–heated cavity. Owing to the axisymmetry of the motion, a streamfunction–vorticity formulation of the meridian flow can be used (see e.g. Reference 19). At the top lid a heat flux is imposed together with a lid velocity. Numerical simulation has been carried out on a 100 × 50 grid. The Reynolds number was 3000 and the Rayleigh number was $7{\cdot}2 \times 10^8$. Figure 10(a) shows the streamline pattern and Figure 10(b) the temperature pattern. This test is a preliminary investigation

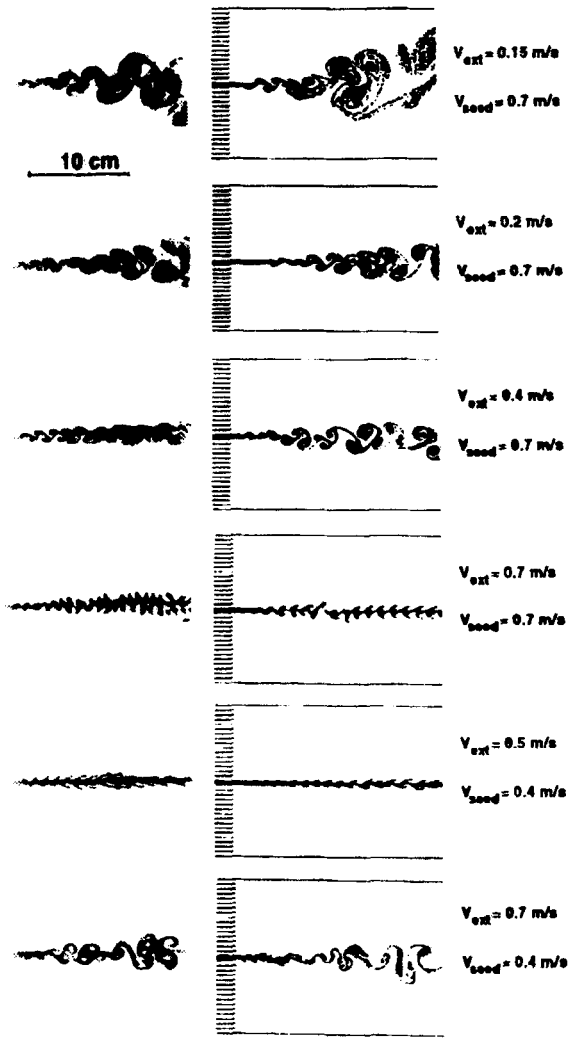

Figure 8. 2D evolving mixing layer. Experimental (left column) versus numerical (right column) simulation

because it is currently analysing the configuration in which natural and forced convection effects are opposite in order to guide the flow to transitional conditions.

4.3. Simulation of compressible complex flows

The compressible two-dimensional Navier–Stokes equations have been solved using an unstructured grid generation technique developed and presented by de Felice *et al.*[20] The choice of an unstructured grid generation is justified by the wide capabilities of such a generation in handling complex geometries (see e.g. References 21 and 22) as well as its adaptive refinement potentialities. In fact,

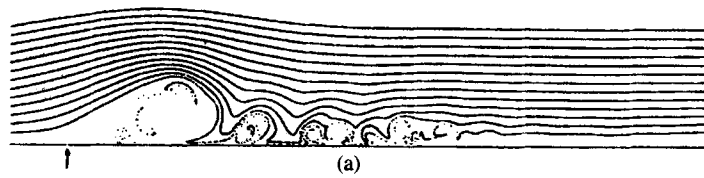

(a)

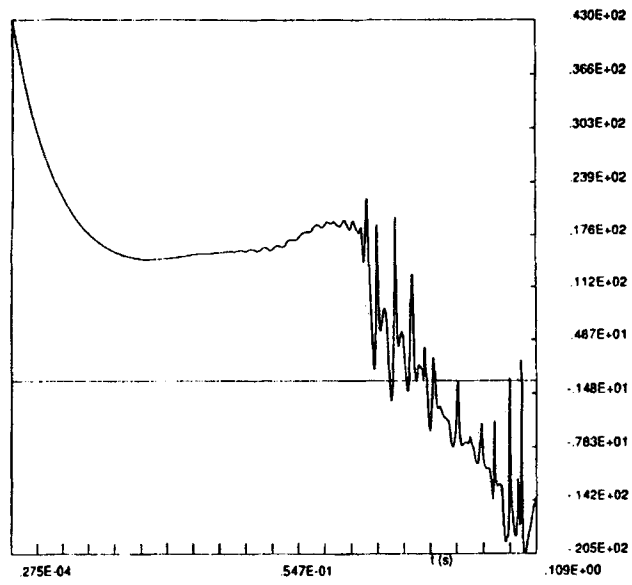

(b)

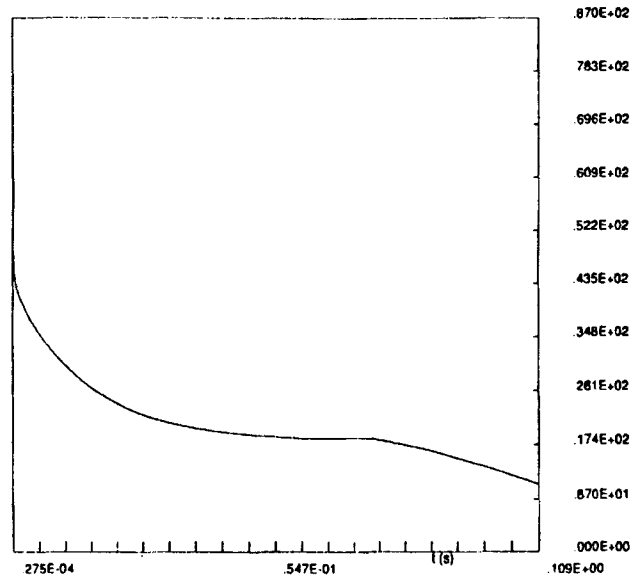

(c)

Figure 9. 2D flow on a flat plate. Effects of transversal slot injection on drag. (a) Streakline pattern. (b) Time evolution of total drag. (c) Time evolution of averaged time integral of total drag

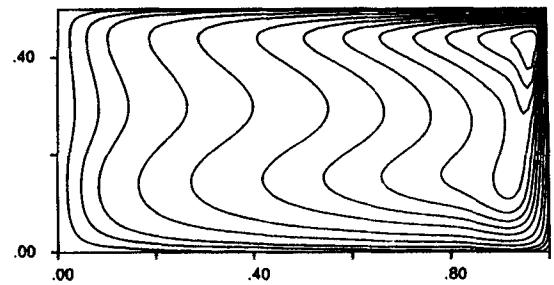

(a)

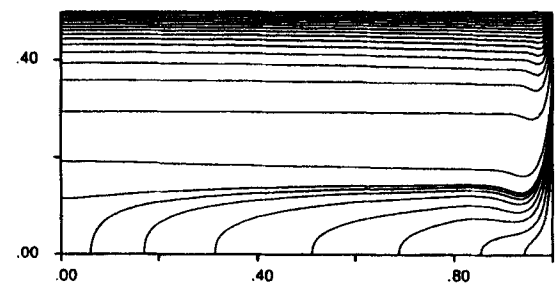

(b)

Figure 10. Axisymmetric rotating–heated cavity. (a) Streamline pattern and (b) temperature contour pattern at $Re = 3000$ and $Ra = 7{\cdot}2 \times 10^8$

relating the local grid size to the transport variables seems to be the best way to locally control the filter function in the present approach. For compressible flows, both DNS (see e.g. Reference 23) and LES (see e.g. Reference 24) approaches can be found in the current literature.

Herein the chosen test is the computation of the flow around a turbine cascade geometry for which the experimental results are available. The system of equations is written in conservative form. A numerical reflecting type of outflow condition was chosen from those proposed in the literature.[23,25–28] In fact, the static pressure at the computational outlet and the stagnation values at the inlet were fixed. With the assigned conditions the estimated Reynolds number referred to the chord length is $2{\cdot}5 \times 10^6$. This flow is particularly critical because the vortex shedding at the trailing edge generates separated flow regions that often cause the failure of most turbulence models. The aim of this simulation is to demonstrate that it is possible to compute the most important part of the flow structures by only resorting to a refinement (i.e. a control of the filter function) of the grid over the shear regions in order to allow an accurate filtering and reconstruction operation of the transport variables. In Figure 11(a) the generated grid (3200 grid points) is shown and in Figure 11(b) the computed isentropic Mach distribution (averaged over an adequate time interval) on the turbine blade is compared with the experimental measurements of Cicatelli *et al.*[29] This comparison shows excellent agreement (about 2

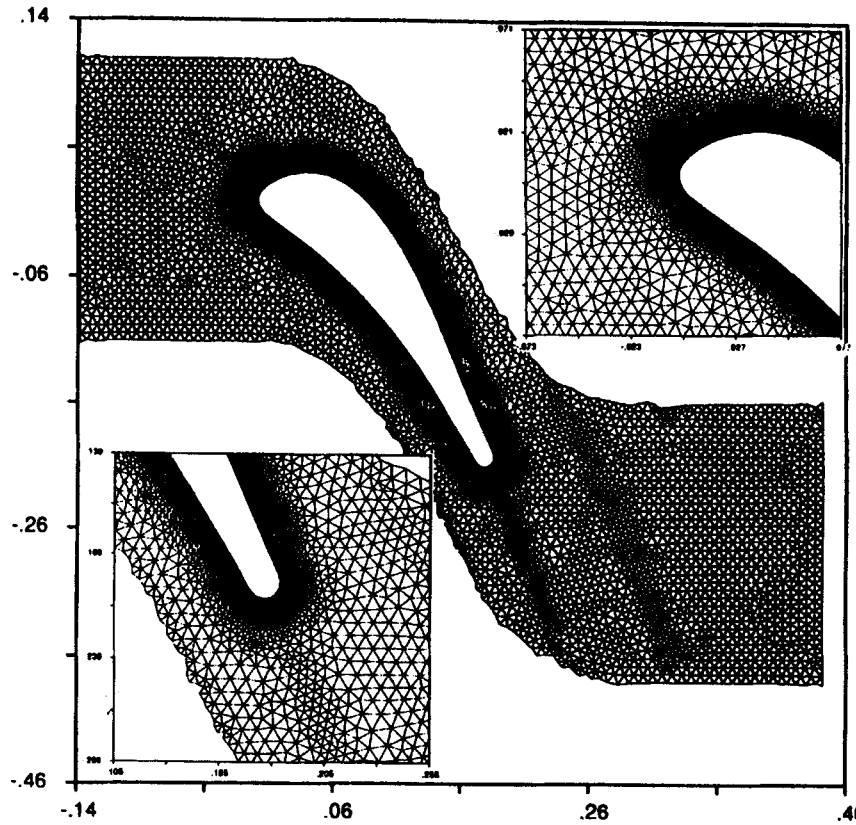

Figure 11(a). 2D compressible flow around a turbine blade. Computational unstructured grid with details of leading and trailing edges

per cent maximum difference) with the experimental measurement. Finally, a streakline pattern is presented in Figure 11(c) where the vortex shedding at the trailing edge and the transport of the large structures clearly appear.

5. DISCUSSION AND CONCLUSIONS

The mathematical background of local average direct numerical simulation (LA-DNS) has been presented. It results in a weak formulation where a transport variable is suitably filtered by means of integration over a control volume.* However, the average operation over a control volume has already been described in some past papers in the form of the so-called 'volume balance procedure'.[30] What is important to remark is the fact that in that early approach the average momentum equations explicitly present the subgrid scale (SGS) Reynolds stresses, i.e. $\overline{\varepsilon_{u_i}\varepsilon_{u_j}} = \overline{u_i u_j} - \overline{u_i}\,\overline{u_j}$, that take the effects of the small scales into account. Actually, it is well known that the source of these stresses is the non-linear advective term and any physical consideration adopted to model them should arise from such nature. Indeed, this has been the guideline of the present work, where the Reynolds stresses are not explicitly

* The main properties we require for the filter function are not discussed because this would be outside the aims of the present paper.

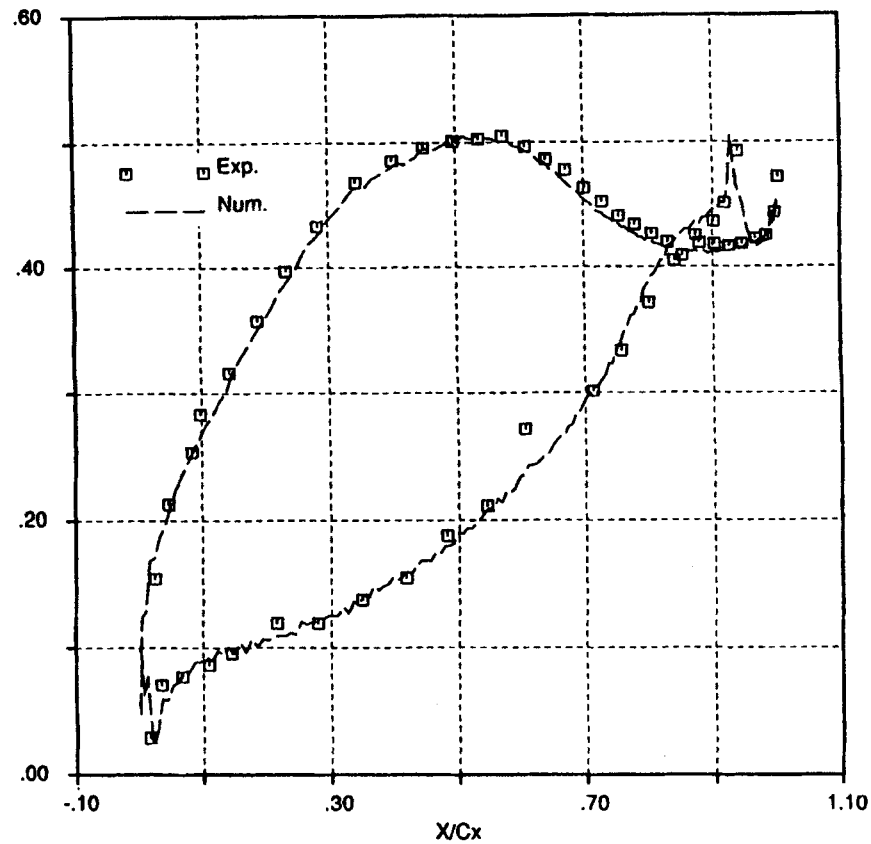

Figure 11(b). 2D compressible flow around a turbine blade. Computed versus experimental isentropic Mach number distribution

extracted from the term $\overline{u_i u_j}$ and therefore are not modelled. In conclusion, highly advective flows can be simulated with a *direct and adequate* treatment of the advective fluxes provided that (i) the filtering is such as to guarantee an accurate discrete representation of the large scale on a given grid and (ii) the reconstruction is such as to make the approximation of the numerical pointwise values (i.e. the set ϕ_i to be considered representative of the transport variable only in some average sense even after the reconstruction) as accurate as possible with respect to the physical local value, i.e. to get $\bar{\varepsilon} \to 0$ for vanishing grid sizes (one remarks that the present filtering operation is such that $\bar{\varepsilon} = \bar{\bar{\phi}} - \bar{\phi}$) at high convergence rate as results from the linear accuracy test-cases. At present the role of the reconstruction step with respect to an SGS closure model has still not been entirely clarified, but it appears quite evident from equation (13) that for suitable values of m and k_ε it results in the formation of an additional eddy viscosity term related to the flow variables and to the computational grid sizes. Finally, the fact that the use of upwinded fluxes should result in very little energy being aliased back owing to the dissipative nature of upwind schemes is noteworthy. On the other hand, whether it can be considered correct to let the scheme assume non-controlled dissipative effects rather than to control them by using explicit models is still controversial.

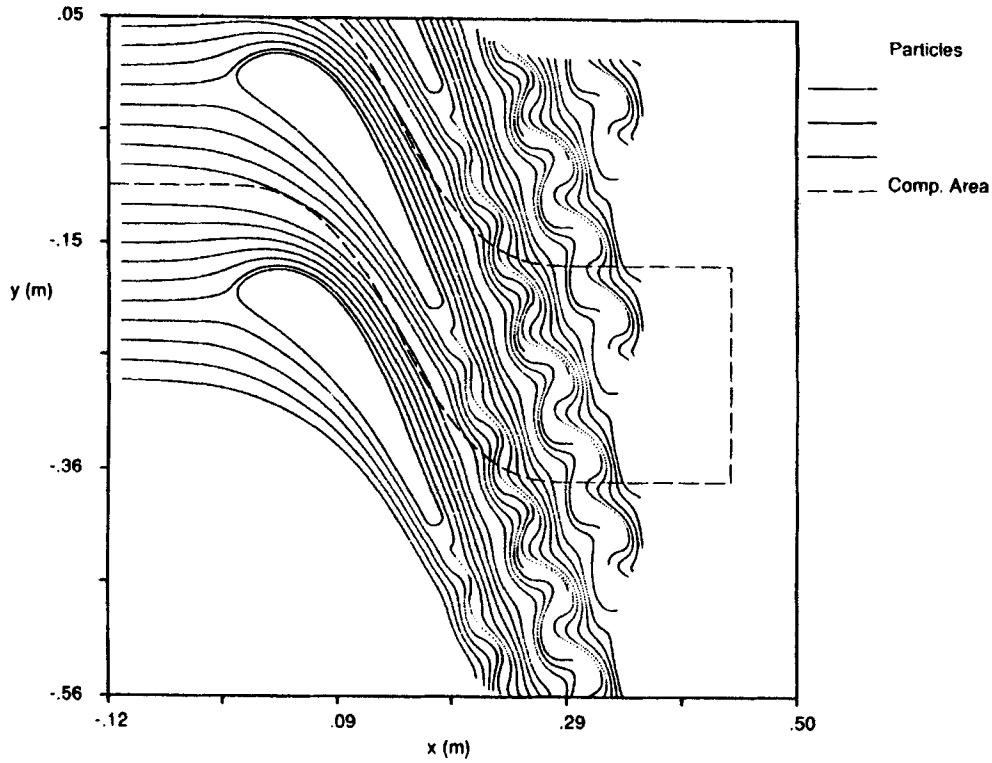

Figure 11(c). 2D compressible flow around a turbine blade. Streakline pattern

The influence of some parameters (the polynomial degree as well as the values of k, m and k_ε) is being studied in order to clarify how the accuracy in replacing a differential operator by a discrete one can influence the approach. Future studies will involve a wide use of unstructured grids for efficient control of the distribution of the filter function over the computational domain as well as a 3D implementation which seems necessary to correctly simulate the flows without 2D assumptions.

ACKNOWLEDGEMENT

This research should be considered as the summa of my research in CFD. I am grateful to Professor C. Meola and Dr. G. de Felice for helping me during my Ph.D. course. I would also like to thank Professor A. Cavaliere for his support and my colleague Dr. F. Sarghini whose contribution in preparing the linear tests and the compressible flow simulation was greatly appreciated.

This research was supported under contract of the Department of Chemical Engineering, University of Naples 'Federico II' during the semester September 1994–February 1995.

REFERENCES

1. J. C. Tannehill, 'Hyperbolic and hyperbolic–parabolic systems', in W. J. Minkowycz, E. M. Sparrow, G. E. Schneider and R. H. Pletcher (eds), *Handbook of Numerical Heat Transfer*, Wiley, New York, 1988, Chap. 12, pp. 463–517.
2. M. M. Ray and P. Moin, 'Direct numerical simulation of transition and turbulence in a spatially evolving boundary layer', *J. Comput. Phys.*, **109**, 169–192 (1993).

3. J. W. Deardorff, 'A numerical study of three-dimensional turbulent channel flow at large Reynolds numbers', *J. Fluid Mech.*, **41**, 453–480 (1970).
4. K. Kuwahara and S. Sharayama, 'Direct simulation of high Reynolds number flows by finite difference methods', in U. Schumann and R. Friedrich (eds), *Notes on Numerical Fluid Mechanics*, Vol. 15, *Direct and Large Eddy Simulation of Turbulence*, Vieweg, Braunschweig, 1985, p. 227.
5. J. Jimenez and P. Moin, 'The minimal flow unit in near-wall turbulence', *J. Fluid Mech.*, **225**, 213–240 (1991).
6. F. M. Denaro, 'Su alcuni schemi alle differenze per la convezione in campo incompressible. Analisi comparativa e nuove proposte', *Graduation Thesis*, University of Naples 'Federico II', 1991.
7. G. de Felice, F. M. Denaro and C. Meola, 'Multidimensional single step vector upwinded schemes for highly convective transport problems', *Numer. Heat Transfer B*, **23**, 425–460 (1993).
8. G. de Felice, F. M. Denaro, C. Meola and F. Sarghini, 'Local average direct numerical simulation of high Reynolds compressible flows based on polynomial upwind schemes on unstructured grids', *J. Fluid Mech.*, submitted.
9. B. P. Leonard, 'Elliptic systems: finite-difference method IV', in W. J. Minkowycz, E. M. Sparrow, G. E. Schneider and R. H. Pletcher (eds), *Handbook of Numerical Heat Transfer*, Wiley, New York, 1988, Chap. 9, pp. 347–378.
10. B. P. Leonard and H. S. Niknafs, 'Sharp monotonic resolution of discontinuities without clipping of narrow extrema', *Comput. Fluids*, **19**, 141–154 (1991).
11. H. Deconinck, R. Struijs, G. Bourgois and P. L. Roe, 'High resolution shock capturing cell vertex advection schemes on unstructured grids', *VKI Lecture Series on Computational Fluid Dynamics, 1994–05*, 1994.
12. J. Casper and H. L. Atkins, 'A finite-volume high-order ENO scheme for two-dimensional hyperbolic systems', *J. Comput. Phys.*, **106**, 62–76 (1993).
13. U. Ghia, K. N. Ghia and C. T. Shin, 'High-*Re* solutions for incompressible flow using the Navier–Stokes equations and multi-grid method', *J. Comput. Phys.*, **48**, 387–411 (1982).
14. M. Deville, T. H. Le and Y. Morchoisne (eds), *Notes on Numerical Fluid Mechanics*, Vol. 36, *Numerical Simulation of 3-D Incompressible Unsteady Viscous Laminar Flows*, 1992.
15. B. F. Armaly, F. Durst, J. C. F. Pereira and B. Schonung, 'Experimental and theoretical investigation of backward-facing step flow', *J. Fluid Mech.*, **127**, 473–496 (1983).
16. L. Schmitt and R. Friedrich, 'Large eddy simulation of turbulent backward facing step flow', in Deville (ed.), *Proc. Seventh GAMM Conf. on Numerical Methods in Fluid Mechanics*, 1987, pp. 355–362.
17. A. Cavaliere, G. de Felice, F. M. Denaro and C. Meola, 'Eulerian and Lagrangian simulation of transport phenomena in multiple or periodical interacting planar jets or wakes versus experimental results', *Proc. 6th Int. Conf. on Computational Methods and Experimental Measurements*, Siena, May 1993, Vol. 1, pp. 135–150, CMP, Southampton and Elsevier, London.
18. F. M. Denaro, B. A. Kolovandin, I. I. Kovaliov and C. Meola, 'Drag reduction and control of boundary layer separation', *J. Eng. Phys. Thermophys.*, submitted.
19. H. J. Lugt and M. Abboud, 'Axisymmetric vortex breakdown with and without temperature effects in a container with a rotating lid', *J. Fluid Mech.*, **179**, 179–299 (1987).
20. G. de Felice, F. M. Denaro, C. Meola and F. S. Sarghini, 'Control volume accurate solution of 2D compressible Navier–Stokes equations on unstructured grid', *Proc. Fifth Int. Conf. of Fluid Mechanics (ICFM5)*, Cairo, January 1995.
21. T. J. Barth and D. C. Jespersen, 'The design and application of upwind schemes on unstructured meshes', *AIAA Paper 89-0366*, 1989.
22. P. Vankeirsbilk and H. Deconinck, 'High order upwind finite volume schemes with ENO properties for general unstructured meshes', *AGARD Rep. R-787*, 1992.
23. T. J. Poinsot and S. K. Lele, 'Boundary conditions for direct simulations of compressible viscous flows', *J. Comput. Phys.*, **101**, 104–129 (1992).
24. G. Erlebacher, M. Y. Hussaini, C. G. Speziale and T. A. Zang, 'Toward the large-eddy simulation of compressible turbulent flows', *J. Fluid Mech.*, **238**, 155–185 (1992).
25. D. H. Rudy and J. C. Strikwerda, 'A nonreflecting outflow boundary condition for subsonic Navier–Stokes calculations', *J. Comput. Phys.*, **36**, 55–70 (1980).
26. K. W. Thompson, 'Time dependent boundary conditions for hyperbolic systems', *J. Comput. Phys.*, **68**, 1–24 (1987).
27. P. Dutt, 'Stable boundary conditions and difference schemes for Navier–Stokes equations', *SIAM J. Numer. Anal.*, **25**, 245 (1988).
28. C. Hirsch, *Numerical Computation of Internal and External Flows*, Vol. 2, *Computational Methods for Inviscid and Viscous Flows*, Wiley, Chichester, 1989, Chap. 19.
29. G. Cicatelli, C. H. Sieverding and N. Feurier, 'Test case 1: Brite turbine blade for time varying wake flow studies', *VKI Lecture Series on Numerical Methods for Flow Calculation in Turbomachines, 1994– 06*, 1994.
30. U. Schumann, 'Subgrid scale model for finite difference simulations of turbulent flows in plane channels and annuli', *J. Comput. Phys.*, **18**, 376–404 (1975).